

# Submarine depression trails driven by the interplay of density currents and fluid migration.

*Maestrelli D.*<sup>1,2</sup>, *Iacopini D.*<sup>3</sup>, *Maselli V.*<sup>3</sup>, *Chiarella, D.*<sup>4</sup>, *Scarselli N.*<sup>4</sup>, *Vannucchi P.*<sup>4,2</sup>, *Jovane L.*<sup>5</sup>,  
*Kneller B.*<sup>3</sup>

<sup>1</sup>Consiglio Nazionale delle Ricerche, Istituto di Geoscienze e Georisorse (CNR-IGG), Via G. La Pira 4, Firenze, Italy

<sup>2</sup>Dipartimento di Scienze della Terra, Università di Pisa, Via S. Maria 53, 56126, Pisa, Italy

<sup>3</sup>Department of Geology and Petroleum Geology, University of Aberdeen, King's college, Aberdeen AB24 3DS, UK

<sup>4</sup>Department of Earth Sciences, Royal Holloway, University of London, Egham Hill, TW20, 0EX, UK

<sup>5</sup>Instituto Oceanográfico, Universidade de São Paulo, Praça do Oceanográfico, 191, 05508-120, São Paulo, Brazil

## Abstract

In this study, we propose a new depositional mechanism for the formation of sea floor depression features similar to pockmark trails, but generated by the interplay between turbidity currents and fluid migration. By using high-resolution 3D seismic data from offshore Ceará State (Brazil), we show how vertically stacked and upslope migrating sediment waves evolve into cyclic steps, promoting the formation of isolated sea floor depressions and, eventually, depression trails. Seismic interpretation and amplitude analysis indicate that the depression trails are very effective not only in shaping the submarine landscape and controlling sediment delivery to the basin but also in creating syn-depositional pathways for vertical fluid migration.

23

24 **Keywords:** sediment waves; fluid migration pathways; density currents; 3D seismic; Brazil

25

## 26 **1. Introduction**

27 The study of fluid migration and accumulation in marine sediments has attracted a large community  
28 of geoscientists due to their importance in predicting the presence of deep-seated hydrocarbon  
29 reservoirs and in understanding the seal capacity and the physical properties of specific stratigraphic  
30 intervals (Hovland, 2003). Trails of circular depressions with a preferred alignment have been  
31 observed in a number of different contexts, some in connection with vertical fluid migration. They  
32 have usually been described as being formed by dewatering of channel fill sands triggered by  
33 overpressure (i.e. pockmarks, Davies, 2003; Pilcher and Argent, 2007) or by turbidity currents that  
34 show streamwise alternations between sub- and super-critical flow regimes (Fildani et al., 2006;  
35 Covault et al., 2014). Heiniö and Davies (2009) described gravity-driven flows interacting with  
36 discontinuities in the topography of deep-sea channels. They showed that turbidity flows were able  
37 to trigger the formation of sediment waves that evolved into circular depressions, termed plunge  
38 pools, with no geophysical evidence of gas-charged sediments or fluid pipes. Vertically stacked  
39 circular depressions have also been observed in the late stage of infill of submarine canyons by Jobe  
40 et al. (2011). In this case, the troughs of a series of cyclic steps generated by dilute turbidity currents  
41 evolve into pockmark fields during the passive infill of the abandoned canyon (Jobe et al., 2011).

42 Here, we use high-resolution 3D seismic data from the offshore Ceará Basin (equatorial Brazil, Fig.  
43 1) to describe a novel sedimentary feature generated by the interplay and mutual feedback between  
44 intermittent fluid flow and long-lasting conditions of sediment supply from turbidity currents. The

45 results obtained will be discussed in the light of better understanding the processes controlling the  
46 evolution of the Brazilian margin but also to presenting a new mechanisms responsible of the  
47 formation of the sea floor topography.

48

## 49 **2. Regional geology and study area**

50 The South Atlantic rift system developed in the Mesozoic time due to the breakup of the Gondwana  
51 super-continent (Morihaq et al., 2000) and is limited to the north by transcurrent fault systems  
52 associated with oceanic fracture zones (the Romanche Fracture Zone, RFZ in Fig. 1) and to the south  
53 by fracture zones in the Malvinas (Falkland) Plateau (MP in Fig.1). The area of interest is considered  
54 part of the Brazilian equatorial margin (Jovine et al, 2016) which opening occurred during the Early  
55 Cretaceous (Neocomian– Barremian; Asmus and Porto, 1972). However due to the presence of a  
56 wide magnetic quiet zone (constant magnetic polarity) from early Aptian to Campanian times,  
57 reconstruction of plate motion during the early drift stage, and the continent-ocean boundary  
58 location are still subjects of a long-lasting debate (Chang et al., 1992).

59 The study area is located in the pull-apart Meso-Cenozoic Ceará Basin in the northern Brazilian  
60 Equatorial passive margin (Fig. 1). Ceará Basin -offshore covers a combined area of approximately  
61 105,000 km<sup>2</sup> and forms the southern flank of the RFZ. The RFZ is a linear fracture zone with an  
62 average width of approximately 16 km that extends over 4500 km from offshore northern equatorial  
63 Brazil to its conjugate margin near offshore Ghana and Togo/Benin. From a tectonic point of view,  
64 the Ceará Basin has three stages of evolution: rift (Neocomian–Eo–Aptian), post-rift (Neoaptian–  
65 Eo–Albian), and continental drift (Albian–Holocene) stages. The rift, post-rift, and continental drift  
66 stages are characterised by continental, transitional, and marine mega-sequence deposits,  
67 respectively (Matos, 1992). The study area extends into the Mondaú sub-basin, part of the Ceará

68 Basin, close to the junction with the Potiguar Basin (Fig. 1). The seafloor lies at about 100 metres  
69 water depth at the shelf edge, dropping to more than 2000 metres toward the continental rise, with  
70 a change of gradient from 1° to more than 3° downslope. Due to the lack of well data, the Neogene  
71 stratigraphy is still pretty elusive. Using our seismic dataset the Neogene stratigraphy can be  
72 subdivided into two main units (Fig. 2): (i) an upper unit (above H1) characterized by a series of  
73 canyons acting as well-developed sediment bypass systems, and (ii) a lower unit (below H1)  
74 characterized by amalgamated channel systems, locally interbedded with mass transport deposits.  
75 From offshore well data (CES-112, Fig. 1) through regional 2D seismic line correlations, the base of  
76 the lower unit has been dated as post upper-Miocene (Jovine et al., 2016).

77 From an oceanographic point of view, the area is characterized by trade winds in the E-NE direction,  
78 with maximum velocity up to 18 m/s (Vital et al., 2010). The North Brazilian Current flows in a W-  
79 NW direction relatively parallel to the coast (Vital et al., 2010; De Almeida et al., 2015). The bottom  
80 currents, which attain velocities of 30–40 cm/s on the shelf, are overlain by tidal and wave  
81 components that are pretty important in triggering shallow low density current (Knoppers et al.,  
82 1999; Vital, 2009).

83

### 84 **3. Dataset and Methods**

85 The dataset from the Ceará Basin consists of a high-quality 3D full stack, Kirchhoff time migrated  
86 reflection seismic volume of ~1600 km<sup>2</sup> acquired by PGS in 2009 (Fig. 1). The line spacing is 12.5 m  
87 in both in-line and cross-line directions. The sample interval is 2 ms (milliseconds). The data are zero-  
88 phase migrated and displayed with Society for Exploration Geologists (SEG) normal polarity, so that  
89 an increase in acoustic impedance is represented by a blue-red-blue reflection loop. The dominant  
90 frequency of the section of interest ranges between 30 and 50 Hz with a vertical resolution of ca.

91 10-18 meters. Velocity values of  $1500 \text{ ms}^{-1}$  have been used for seawater and 1800 to  $2500 \text{ ms}^{-1}$  for  
92 the studied interval from the nearest (2 km to the SE) well CE-112 (Fig. 1; Conde et al., 2007).  
93 Structural maps of key horizons were generated from a subset of the data (seabed in Fig. 1, Fig. 3),  
94 using a combination of two seismic attributes (root mean square of amplitude, and variance; Chopra  
95 & Marfurt, 2007). Finally, a qualitative amplitude versus offset (AVO) analysis (Castagna et al., 1998)  
96 using partial stack data imaging a portion of the seismic area has been applied to investigate the  
97 significance of some of the bright and weak anomalies affecting the depression trails. The partial  
98 stacks have been processed following a robust workflow for amplitude preservation and noise  
99 suppression (see supplementary material).

100

## 101 **4. Results: sedimentary architectures and amplitude anomalies**

### 102 **4.1. Sedimentary architecture**

103 In the upper slope region of the study area, the sea floor is characterized by fields of sediment waves  
104 (SW) with an upslope direction of migration, showing a wavelength of about 250 meters and a  
105 height of 10-50 metres (Fig. 2a, and Fig. 4). The sediment waves evolve downslope into circular to  
106 elliptical depressions with a maximum diameter of 1 km (Figs. 1 and 4), maximum depth of 300 m  
107 with asymmetric internal flanks (Figs. 2a, c). These depressions occur either isolated, recalling the  
108 geometry of pockmarks (arrow 1 in Fig. 2b, Fig. 4), or in trails aligned downslope and often merging  
109 together (arrow 2, Fig. 2b), developing a more elongated (channel-like) composite morphology  
110 (arrow 3 in Fig. 2b, Fig. 4). Seismic reflection profiles reveal that in the subsurface (Fig. 2) these  
111 features develop as a series of vertically-stacked concave-up units, characterized by variable  
112 amplitude. These concave-up structures represent the troughs of vertically stacked depressions (Fig.  
113 2a) and are characterized by minor erosional surfaces (red dotted line, Fig. 2b) and truncated

114 reflections (arrow 2 in Fig. 2b), bounded by continuous horizons (H2, H3, Fig. 2d). In plan view, the  
115 vertically stacked concave-up structures highlighted in Figure 2b appear as sub-circular features  
116 (green arrow in Fig. 3), but also isolated depressions (Fig. 4). Some of these features extend from  
117 the basal horizon (H2) up to the sea floor, maintaining almost the same position and finally  
118 appearing as a depression on the seabed (Fig. 2c). Other examples are filled by sub-horizontal units  
119 that onlap the concave-upwards bounding surface, leaving them with no expression on the seafloor  
120 (Fig 2d). Mapped seismic horizons (named H1 to H3 from deep to shallow, Fig. 3) across the Neogene  
121 units reveal the following key information: a) embryonic channel features observed in H1 (Fig. 3)  
122 representing the precursors to the main active channels currently observed on the seafloor (SB in  
123 Fig. 3); b) the mapped seismic horizons H1 to H3 (Fig. 3) show that the embryonic channel  
124 consistently behaved as an erosion-prone feature through time, while the inter-channel aggraded  
125 continuously; c) both isolated depressions and linear arrays of depressions are observed across the  
126 entire area, along the channel and beyond along the inter-channel (H1-H3 in Fig. 3). The recently  
127 active channel has deep erosive walls, 200-300 meters high, with little or no evidence of overspill  
128 deposit (Fig. 4).

129 At a closer scale of observation (Figs. 2b, d), stacking of concave reflections shows that they develop  
130 as a set of aggrading packages, with the troughs of each package displaced either sub-vertically or  
131 upslope from the previous one (Figs. 2c, d). Each package is commonly separated from the following  
132 one by a draping unit (when not eroded) observed inside the depression (Figs. 2b, c). Furthermore,  
133 horizons H1, H2 and H3 can be traced in the entire dataset and probably originated during periods  
134 of reduced turbidity current activity and increased pelagic/hemipelagic deposition draping both  
135 depressions and abandoned canyons (green arrow in H3, Fig. 3). While at the seabed and in the  
136 subsurface some of the depression trails appear isolated, many others are localized along the axis  
137 of the canyon, resulting in a stepped pattern evident in both buried and active canyons (Figs. 2c and

138 3 H1 to SB). Finally, the most notable feature is the correspondence between the centres of the  
139 depressions and the brightness of some reflectors within them (localised positive and negative weak  
140 to bright amplitude anomalies) as shown in figures 2b, c and d.

141

#### 142 **4.2. Amplitude anomalies across trough structures:**

143 In the studied dataset, there is a clear correspondence between stacked positive bright amplitudes  
144 (arrows 1 and 3 in Fig. 2b), negative bright amplitude (arrows 4 and 5 in Fig. 2c), and depressions  
145 (arrows in Figs. 2b to d). Several troughs are also characterized by the presence of a flat spot (see  
146 arrows 9 and 10 above H3, Fig. 3c) lying inside the buried depressions within the passive infill of the  
147 depressions. In detail, the amplitude brightness within the trough structures (Figs. 2b, c and d)  
148 indicates the following trend:

- 149 - In Figure 2b, stacked positive anomalies with weaker amplitude than the seabed are  
150 observed through the fill of the trough from bottom to top (arrows 1 and 2). In some cases,  
151 clear flat spot (arrows 3) with a concordant polarity to the seabed appear in the apparently  
152 passive infill.
- 153 - In Figure 2c, we observe clear depressions onto the seafloor, both affected by weak to strong  
154 (arrow 5) negative anomalies.
- 155 - In Figure 2d, weak bright anomalies with contrasting polarity to the seabed (arrows 8 and 9)  
156 are observed also across the aggrading trough. Arrows 6 and 10 shows soft flat spots within  
157 the infill. Between trough trails, by contrast, strong negative bright spots are present (arrow  
158 7).

159 AVO analysis, performed using partial stack imaging of some of the flat spots (Figs. 5a and c) and  
160 plotted in gradient versus reflectivity (intercept) diagram (Fig. 5b) indicates that the weak positive

161 amplitude anomalies (observed distributed across the depression trails, Fig 5c) show a lateral spread  
162 (green triangle) along the background distribution but with a weak change in fluid saturation or  
163 shale content (as indicated by the red arrows in Fig 5b). We do not observe any clear distinctive  
164 trend toward the negative reflectivity and negative gradient quadrant.

165

## 166 **5. Discussion: a model for the depression trails and fluid migration pathways**

### 167 **5.1. Amplitude anomalies and trough structures**

168 In seismic reflection data, isolated bright spots (regardless of the polarity) commonly suggest a  
169 change in the grain size or cementation of the sediment, and/or the presence of fluid with properties  
170 significantly different from normal saline pore water (Asveth et al., 2013; and references therein).  
171 Below the seabed, where sand is poorly consolidated, the negative amplitude anomalies may well  
172 indicate presence of gas fluid (Asveth et al., 2013). On the other hand, weak positive amplitude  
173 anomalies affecting the troughs (Fig. 2c) are more ambiguous and cannot be unequivocally  
174 associated with fluid (Asveth et al., 2013) but rather to either sediment cementation or grain size  
175 changes.

176 The plotted AVO analysis (see supplementary material) in a diagram gradient versus intercept (Fig.  
177 5) confirms the ambiguity of those anomalies, as no clear distribution trend (versus the lower or  
178 both negative gradient and intercept quadrant of the diagram) typical of gas fluid is observed. The  
179 green points clearly distribute and scatter along the main diagonal brine sand background with no  
180 or a minimal deviation respect to it (Fig. 5b).

181 In particular, these stacked weak amplitude anomalies at the concave base of the structures may  
182 instead suggest:



- 183 a) Vertical variation of grain size and cementation (and consequently porosity and  
184 permeability) within the troughs of these depressions (weak positive anomalies, Figs. 2b and  
185 d);
- 186 b) Fluid presence within the vertically stacked depression, perhaps facilitated by their  
187 petrophysical characteristics (increased porosity and permeability), (negative amplitude  
188 anomalies, Fig. 2c).

189 Field evidences from different depositional settings prove the importance of unidirectional flows –  
190 both bottom currents and subsurface fluid migration – in the reorganization of surface and  
191 subsurface sediments (Gong et al., 2012). Accumulation of coarse-grained and porous sediment  
192 related to the vertical aggradation of consecutive depressions may explain both the weak positive  
193 amplitude anomalies produced by variation of porosity/granulometry and preferential cementation  
194 along the trough of the depressions (Fig. 2d). In areas saturated by fluid such grain size variation  
195 might also promote and localize preferential pathways for fluid migration (Fig. 2c). The bright  
196 negative amplitude anomalies observed all along the troughs in Figure 2c (arrows 4 and 5) might  
197 indeed represent active fluid pathways exploiting the concave depression structure all the way up  
198 to the seabed. However, following the above considerations figures 2b and 2d seem to suggest that  
199 the positive amplitudes across the troughs (arrows 1 to 3) are expressions solely of grain-size  
200 variations and cementation effects.

201

## 202 **5.2. Down-slope arrays that nucleated the ‘canyons’**

203 Following the all previous observations, we infer that the extensive field of circular depressions was  
204 initiated (H1, green reflector in Figs. 2 and 3) as a series of sediment waves (SW in Fig. 2a) related  
205 to periodic instabilities generated by unconfined and low density gravity currents (LDGf in Fig. 2a;

206 arrow 4 in Fig. 2; green arrows in Fig. 4; Lesshafft et al., 2011), commonly generated by the impact  
207 of storm waves on the outer shelf and upper slope (Mulder et al., 2001; Puig et al., 2004;). These  
208 may interact with span-wise instabilities (Hall et al., 2008) to generate the observed randomly  
209 distributed depressions on the slope (Fig. 2 S1, Fig. 3 H1), and led to coalescence of some of these  
210 depressions into systematic downslope arrays (Fig. 2, arrows 2 and 3). These appear to have been  
211 amplified and perpetuated as cyclic steps (Cartigny et al., 2011; CS in Fig. 2a and 4), features that  
212 have been recognized in many submarine canyons and channel systems (Normark et al., 2002;  
213 Symons et al., 2016).

214 The conceptual diagram in Figure 6 presents an evolutionary sequence for these shallow structures.  
215 Each depression evolves in two more or less distinct stages.

216 (a) Preferential sea-floor erosion (truncation of seismic reflectors) amplifying the depressions  
217 (Fig. 6, T1);

218 (b) Partial fill of the depression, shown by onlapping seismic reflectors of varying amplitude,  
219 and with geometries ranging from planar and horizontal with abrupt onlap (Fig. 2b, arrows  
220 2 and 3) to concave-upwards with only slight thickening into the base of the depression (Fig.  
221 2b, arrow 1; Fig. 2c arrows 4 and 5, Fig. 6, T2 to T3).

222 We relate sea-floor erosion to the formation of cyclic steps (clearly visible in figures 2a and 3) by  
223 bypassing of turbidity currents along the pathways created by coalesced depressions. The more  
224 isolated depressions experienced less (if any) erosion (Figs. 2c and 3, SB), being off the main fairway.  
225 Flat, high-amplitude fill is found within the continuous downslope arrays of depressions, and thus  
226 occurs in areas of prior erosion which, we surmise, is an indication of more energetic and perhaps  
227 coarser-grained and higher-density turbidity currents (e.g. Talling et al., 2012). In contrast, the  
228 concave-upwards fills, which tend to show only relatively slight thickening into the depression,

229 suggests lower density, finer-grained turbidity currents, moving downslope away from the main  
230 sediment fairway. These interpretations are consistent with our interpretation of the amplitudes.

231

### 232 **5.3. Depression trail and fluid pathway**

233 A detailed analysis of the seismic amplitude across the entire sequence clearly shows that the  
234 concave up fills of both isolated troughs and depression trails are affected by weak to bright  
235 amplitude anomalies from bottom to top. In some cases (Fig. 2c) the concave-upward fills (with  
236 slight thickening into the depressions) show weak to strong negative anomalies suggesting the  
237 presence of fluid affecting the trough. In other cases (Fig. 2d), flat high amplitude fills can be  
238 observed along the depression trail. The negative amplitude indicates the presence of fluid either  
239 still sealed by the draping unit (arrows 9 and 10 in Fig. 2d) or leaking to the surface (arrow 4 in Fig.  
240 2d); while the positive amplitude may suggest a grain size or cementation effect (footprint of past  
241 fluid deposition). In both cases, the bright anomalies within the troughs may either represent the  
242 presence of (or a pathway for) fluid, or the presence of coarser grained sediment. Finally, the clear  
243 onlapping nature of the main bright infill and flat spot onto the erosive surface suggests that fluid  
244 may have migrated and/or been trapped during the cyclic erosional and depositional evolution of  
245 the trough. This allows us to infer that the depression trails may have acted as preferential pathways  
246 for syn-depositional vertical fluid migration. Therefore the evolution of the depression trails might  
247 include a punctuated interaction between turbidity currents and fluid flow to the sea-floor,  
248 generating re-suspension of fine sediments, producing a passive enrichment in coarser fractions  
249 during the upslope migration and stacking of the troughs of these cyclic steps (Fig. 4 T2 to T3).

250

## 251 **6. Conclusions**

252 We describe a dispersed distribution of seafloor depressions that resemble classical pockmarks.  
253 Their internal architecture and reflection configuration support the hypothesis that these trails of  
254 depressions are generated by upslope migrating cyclic steps produced by gravity-driven flows.  
255 Amplitude analysis across the depression trails indicates that fluids may exploit pathways generated  
256 by the troughs of these vertically stacked depressions or cyclic steps. The interaction between  
257 turbidity currents and fluid flow might generate re-suspension of fine sediments, producing a  
258 passive enrichment in coarser fractions and the upslope migration and stacking of the troughs of  
259 these features. Our observations suggest that the interplay between slope sedimentation and fluid  
260 flow may represent a key process in shaping the seafloor of many slope settings worldwide.

261

## 262 **Acknowledgments**

263 We sincerely thank Petroleum Geo-Services (PGS), CGG and specifically David Hajovsky and C. Baron  
264 who kindly furnished the dataset and allowed us to show these results. We are grateful to Huuse,  
265 Duarte for their constructive comments of a previous draft. D.M. was funded through the Tuscany  
266 PhD Regional program [grant POR ICO FSE 2014/2020-Asse C] and the Erasmus+ exchange for his  
267 visit in Aberdeen.

268

## 269 **Declaration of interest**

270 Declarations of interest: none.

271

272

273

274 **References**

- 275 Almeida, N.M. Vital, H.,Gomes, M.P. 2015. Morphology of submarine canyons along the continental  
276 margin of the Potuigar Basin , NE Brazil. *Marine and Petroleum Geology* 68, 307-324
- 277 Asmus, H.E. , Porto R. 1972. Classification of Brazilian sedimentary basins according to plate tectonics.  
278 Congresso Brasileiro de Geologia 26, Belém (Ed.), Anais do XXVI Congresso Brasileiro de  
279 Geologia, 2, Sociedade Brasileira de Geologia, São Paulo (1972), pp. 67-90. (in Portuguese).
- 280 Avseth,P., Mukerji, T. and Mavko G. 2005. Quantitative seismic interpretation. Cambridge Press.
- 281
- 282 Cartigny, M.B., Postma, G., van den Berg, J.H., and Mastbergen, D.R., 2011. A comparative study of  
283 sediment waves and cyclic steps based on geometries, internal structure and numerical  
284 modelling. *Marine Geology* 280, 40-56. <https://doi.org/10.1016/j.margeo.2010.11.006>
- 285 Cartwright J. and Santamarina, C., 2015. Seismic characteristics of fluid escape pipes in sedimentary  
286 basins: Implications for pipe genesis. *Marine and Petroleum Geology*, 65, 126-140.  
287 <https://doi.org/10.1016/j.marpetgeo.2015.03.023>
- 288 J.P. Castagna, H.W. Swan, D.J. Foster. Framework for AVO gradient and intercept interpretation.  
289 1998. *Geophysics*, 63, 948-956.
- 290 Chang, H.K., R. O. Kowsmann, A. M. F. Figueiredo, and A. A. Bender, 1992. Tectonic and stratigraphy  
291 of the East Brazil Rift system: an overview. *Tectonophysics*, 213, 97-138.
- 292 Covault, J.A., Kostic, S., Paull, C.K., Ryan, H.F., Fildani, A., 2014. Submarine channel initiation, filling  
293 and maintenance from sea-floor geomorphology and morphodynamic modelling of cyclic  
294 steps. *Sedimentology* 61, 1031-1054.

295 Davies, R. J., 2003. Kilometer-scale fluidization structures formed during early burial of a deep-water  
296 slope channel on the Niger Delta. *Geology*, 31-11, 949-952.  
297 <https://doi.org/10.1130/G19835.1>

298 Gong, C., Wang, Y., Peng, X., Li, W., Qiu, Y., and Xu, S., 2012. Sediment waves on the South China  
299 Sea Slope off southern Taiwan: Implications for the intrusion of the Northern Pacific Deep  
300 Water into the South China Sea. *Marine and Petroleum Geology* 32, 95-109.  
301 <https://doi.org/10.1016/j.marpetgeo.2011.12.005>

302 Hall, B., Meiburg, E. and Kneller, B., 2008. Channel formation by turbidity currents: Navier–Stokes-  
303 based linear stability analysis. *Journal of Fluid Mechanics*, 615, pp.185-210.

304 Heiniö, P., and Davies, R.J., 2009. Trails of depressions and sediment waves along submarine  
305 channels on the continental margin of Espirito Santo Basin, Brazil. *Geological Society of  
306 America Bulletin* 121, 698-711. <https://doi.org/10.1130/B26190.1>

307 Ho, S., Cartwright, J., and Imbert, P., 2012. The Formation of advancing pockmarks arrays: an  
308 interplay between hydrocarbon leakage and slope sedimentation. AAPG Annual Convention  
309 and Exhibition, Long Beach California, April 22-25.

310 Hovland, M., 2003. Geomorphological, geophysical, and geochemical evidence of fluid flow through  
311 the seabed. *J. Geochem. Exploration*, 78-79, 287-291

312 Jobe, Z. R., Lowe, D. R., and Uchytíl, S. J., 2011. Two fundamentally different types of submarine  
313 canyons along the continental margin of Equatorial Guinea. *Marine and Petroleum Geology*,  
314 28(3), 843-860. <https://doi.org/10.1016/j.marpetgeo.2010.07.012>

315 Judd, A., and Hovland, M., 2009. Seabed fluid flow: the impact on geology, biology and the marine  
316 environment. Cambridge University Press. New York, 492 pp

- 317 Knoppers, B., Ekau, W., Figueiredo, A.G., 1999. The coast and shelf of east and northeast Brazil and  
318 material transport. *Geo Mar. Lett.*, 19, pp. 171-178
- 319 Lesshafft, L., Hall, B., Meiburg, E. and Kneller, B., 2011. Deep-water sediment wave formation: linear  
320 stability analysis of coupled flow/bed interaction. *Journal of Fluid Mechanics*, 680, pp.435-  
321 458.
- 322 Matos, R.M.D., 2000. Tectonic evolution of the equatorial South Atlantic. W.U. Mohriak, M. Talwani  
323 (Eds.), *Atlantic Rifts and Continental Margins*, Geophysical Monograph, 115, American  
324 Geophysical Union . 331-354
- 325 Mohriak, W.U., M. Basseto, and I.S Vieira, 2000. Tectonic Evolution of the Rifted Basins in the  
326 Northeastern Brazilian Region. In: W.Mohriak and M.Talwani, eds., *Atlantic Rifts and*  
327 *Continental Margins: Geophysical Monograph 115*, 293-315.
- 328 Mulder, T., Weber, O., Anschutz, P., Jorissen, F., and Jouanneau, J.M., 2001. A few months-old  
329 storm-generated turbidite deposited in the Capbreton Canyon (Bay of Biscay, SW France).  
330 *Geo-Marine Letters*, 21(3), 149-156. doi:10.1007/s003670100077
- 331 Normark, W.R., Piper, D.J., Posamentier, H., Pirmez, C., and Migeon, S., 2002. Variability in form and  
332 growth of sediment waves on turbidite channel levees. *Marine Geology* 192, 23-58.  
333 [https://doi.org/10.1016/S0025-3227\(02\)00548-0](https://doi.org/10.1016/S0025-3227(02)00548-0)
- 334 Osborne, M. J., and Swarbrick, R. E., 1997. Mechanisms for generating overpressure in sedimentary  
335 basins: a reevaluation. *AAPG bulletin*, 81(6), 1023-1041.
- 336 Pilcher, R., and Argent, J., 2007. Mega-pockmarks and linear pockmark trains on the West African  
337 continental margin. *Marine Geology* 244, 15-32.

338 Puig, P., Ogston, A. S., Mullenbach, B. L., Nittrouer, C. A., Parsons, J. D., and Sternberg, R. W., 2004.  
339 Storm-induced sediment gravity flows at the head of the Eel submarine canyon, northern  
340 California margin. *Journal of Geophysical Research: Oceans*, 109(C3).  
341 doi:10.1029/2003JC001918.

342 Szatmari, P. , Françolin, J.B.L. , Zanotto, O., Wolff, S. 1987. Tectonic evolution of the Brazilian  
343 equatorial margin *Rev. Bras. Geociênc.*, 17, 180-188. (in Portuguese)

344 Symons, W. O., Sumner, E. J., Talling, P. J., Cartigny, M. J., and Clare, M. A., 2016. Large-scale  
345 sediment waves and scours on the modern seafloor and their implications for the prevalence  
346 of supercritical flows. *Marine Geology*, 371, 130-148.  
347 <https://doi.org/10.1016/j.margeo.2015.11.009>

348 Talling, P.J., Masson, D.G., Sumner, E.J. and Malgesini, G., 2012. Subaqueous sediment density flows:  
349 Depositional processes and deposit types. *Sedimentology*, 59, 1937-2003.

350 Vital, H. 2009. The mesotidal barriers of Rio Grande do Norte. S. Dillemburg, P. Hesp (Eds.), *Geology*  
351 *of Brazilian Holocene Coastal Barriers*, Springer-Verlag, Heidelberg, pp. 289-324  
352

353 Vital, H. Gomes, M.P., Tabosa, W.F., Frazao, E.P, Santos, C.L.A., Placido Junior. J.S. 2010.  
354 Characterization of the Brazilian Continental shelf adjacent to Rio Grande do Norte State, NE  
355 Brazil. *Braz. J. Oceanogr.*, 58, 43-54

356

357

358

359

360



361 **Figure captions**

362 **Figure 1.** The study area, offshore of Ceará state (Brazil). The white polygon represents the dataset,  
363 while the red rectangle marks the area from where examples shown in this paper come. The blue  
364 surface represents the fully mapped seabed. Arrow 1: isolated pockmark-like structure; Arrow 2:  
365 depression trails aligned parallel to the sea floor gradient; Arrow 3: elongated channel-like  
366 morphology; Arrow 4: roughness of the paleo-sea floor triggered by the impact of storm waves.

367

368 **Figure 2.** (a) 3D seismic block showing the depressions at the seabed, the turbidite channel and the  
369 smaller canyons. Inside this latter are visible depressions-stepped pattern, generated by sediment  
370 waves (SW) and cyclic steps (CS). LDGf: Low Density Gravity flow; FM: Fluid Migration. (b) A crossline  
371 (A-B) showing stacked depressions culminating in pockmark-shaped depressions at the seafloor. (c)  
372 Stacked bright soft anomalies (Arrows 4 and 5) affecting two main depressions both emerging on  
373 the seafloor. (d) Section CD (inline) showing buried stacked depressions. Arrows 6 and 9 represents  
374 soft (negative) amplitude bright anomalies (arrow 9 as a flat spot). Arrows 7 and 10 shows weak to  
375 hard anomalies concordant with the seafloor. Seismic section traces are reported in Figure 3 (H3).  
376 Red arrows in b, c and d indicate bright anomalies across the trough.

377

378 **Figure 3.** The mapped key horizons H1, H2, H3 and the seabed (SB). Yellow boundaries highlight the  
379 position of the turbidite channels. Section AB, CD and EF represent the images shown in Figure 2.

380

381

382

383 **Figure 4.** Portion of the mapped seabed highlighting the presence of canyons, turbidite channels  
384 and widely distributed pockmark-shaped depressions. LDGf: Low Density Gravity flow; HDGf: High  
385 Density Gravity flow

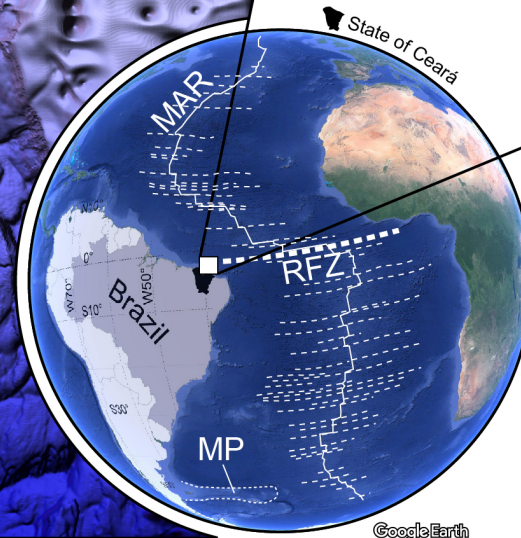
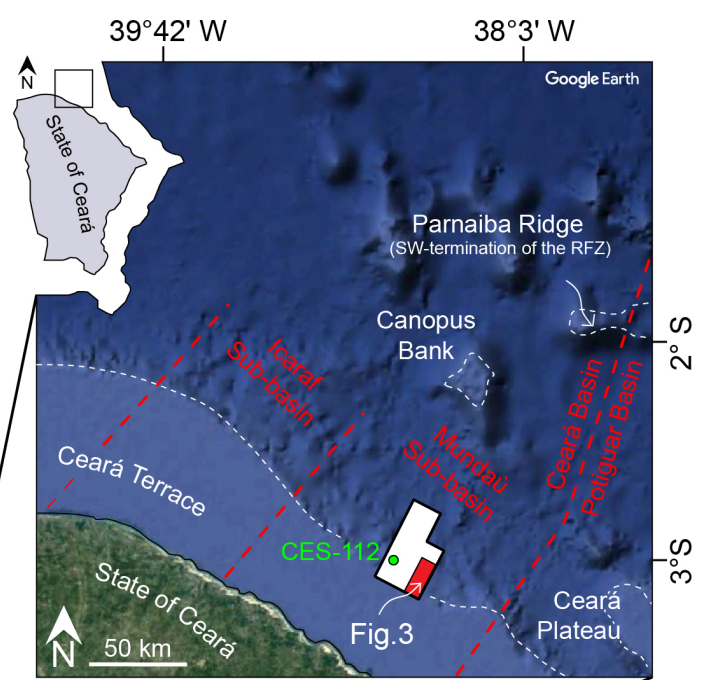
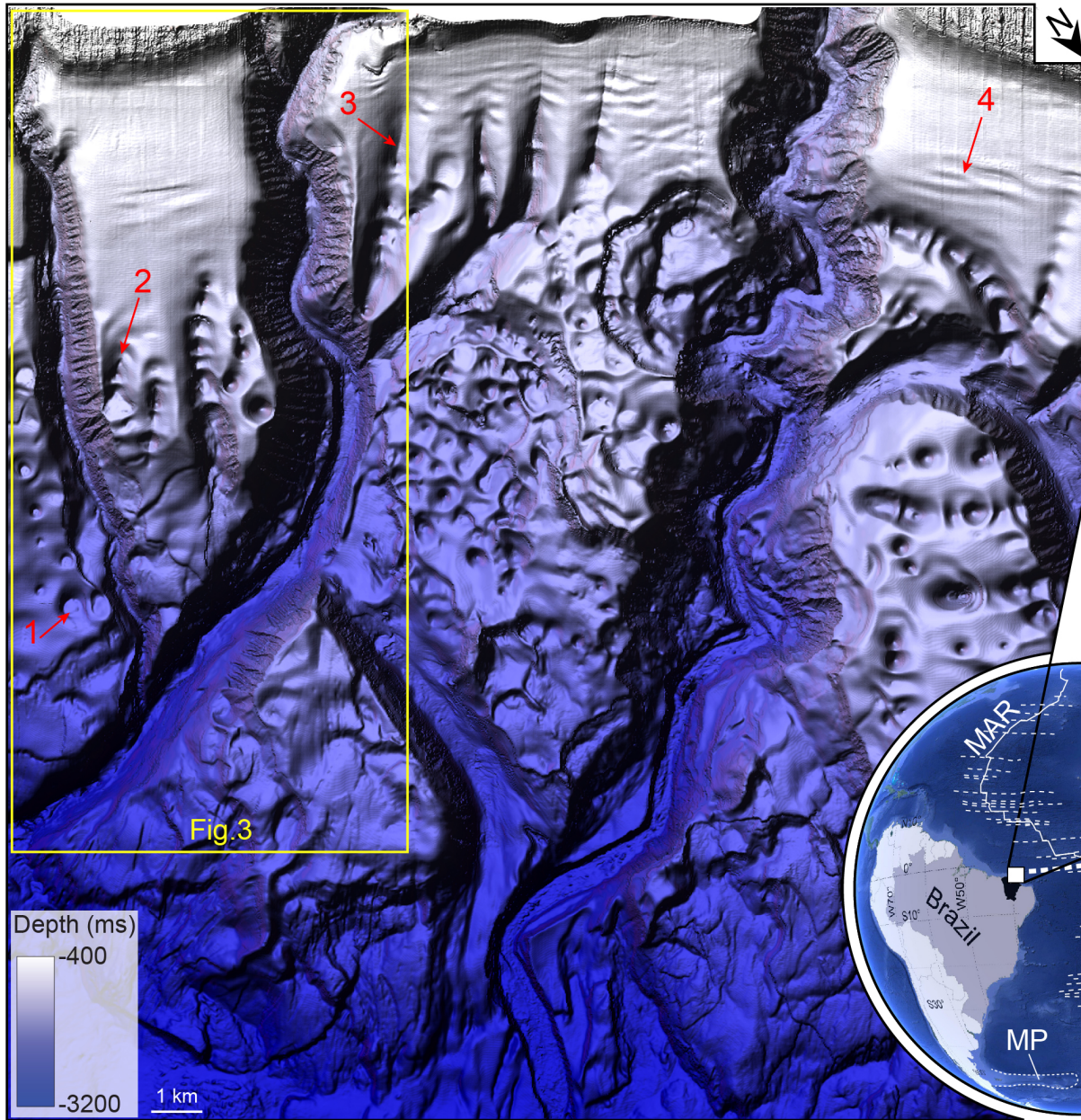
386





387 **Figure 5:** AVO analysis using partial stack from a section of the investigation area. (a) Location of the  
388 3D seismic dataset (CGG Ceara basin, partial stack) , Ceara basin. (b) Gradient versus intercept  
389 crossplot of the amplitude selected from Figure 5c. In blue triangle are the normal amplitude brine  
390 sand defining the background trend. In green, the weak positive bright green amplitude selected  
391 from Figure 5c. Notice the poor/weak fluid factor effect suggesting a non-hydrocarbon effect in  
392 controlling the brightness. It indicates that the weak positive amplitude anomalies observed across  
393 the depression trails do shows a possible changes in fluid saturation or shale content but with no  
394 regard to the typical gas or hydrocarbon anomaly AVO classes (Avseth et al.,2005). (c) Seismic  
395 section showing the selected area under analysis: in green the weak brightness from the depression  
396 trough; in blue the sand.

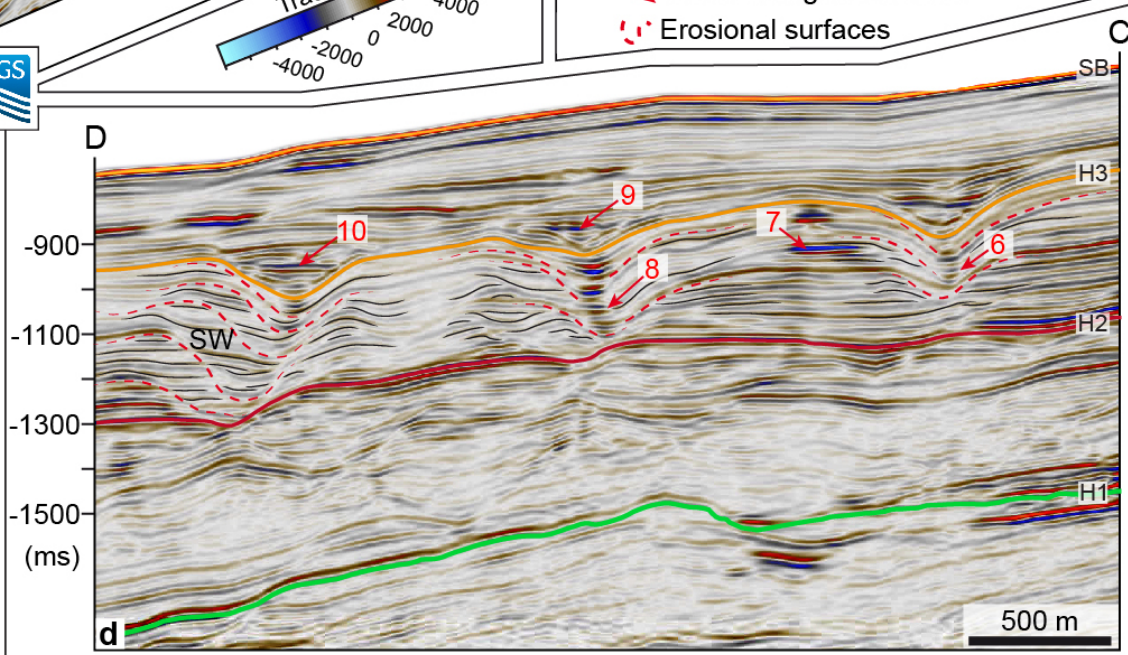
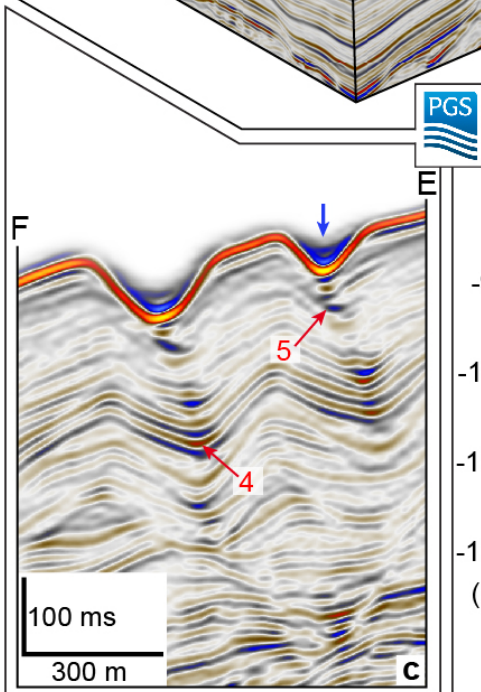
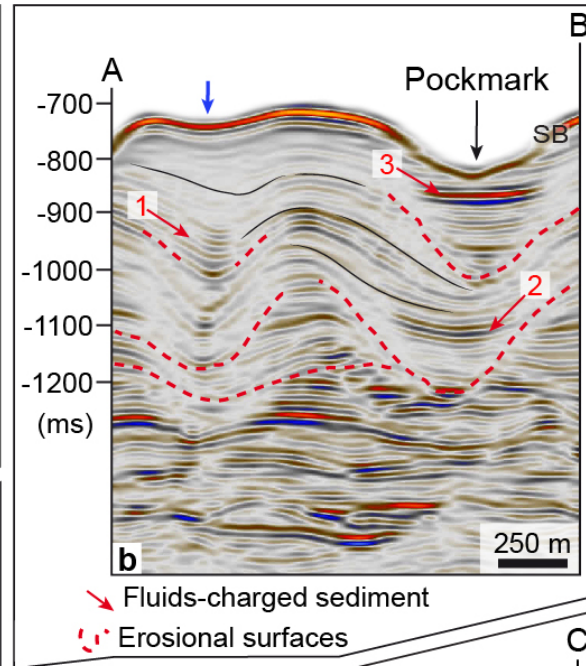
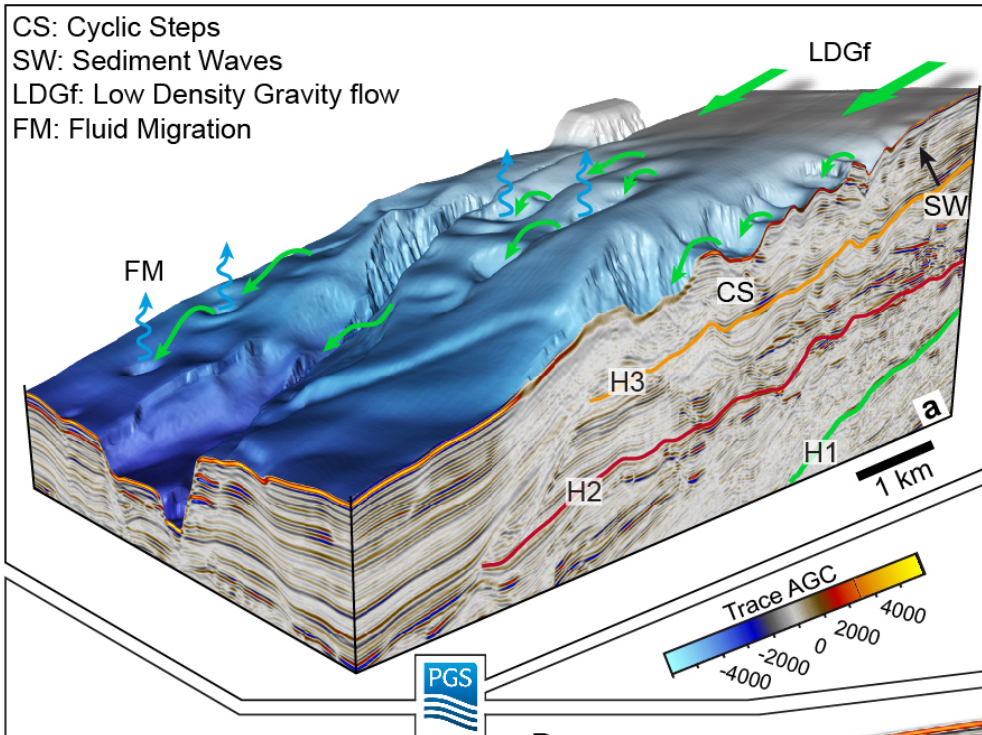
397

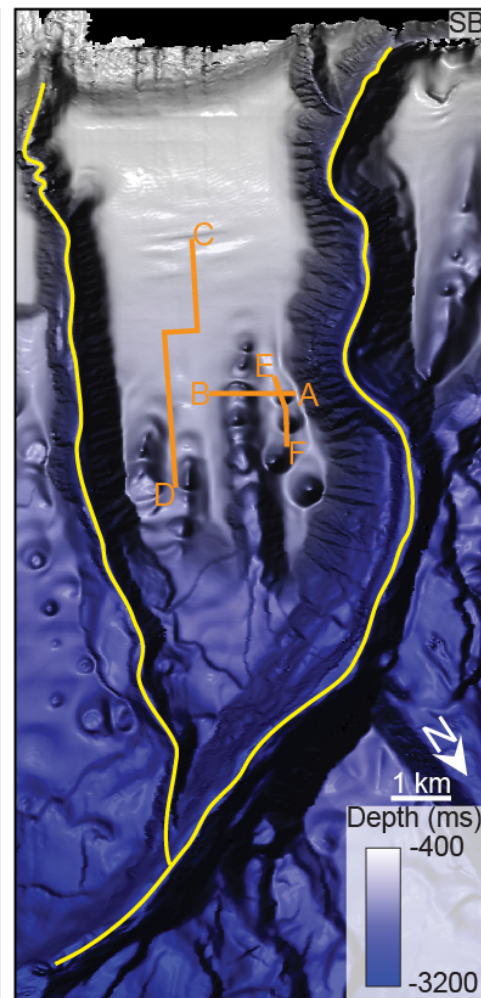
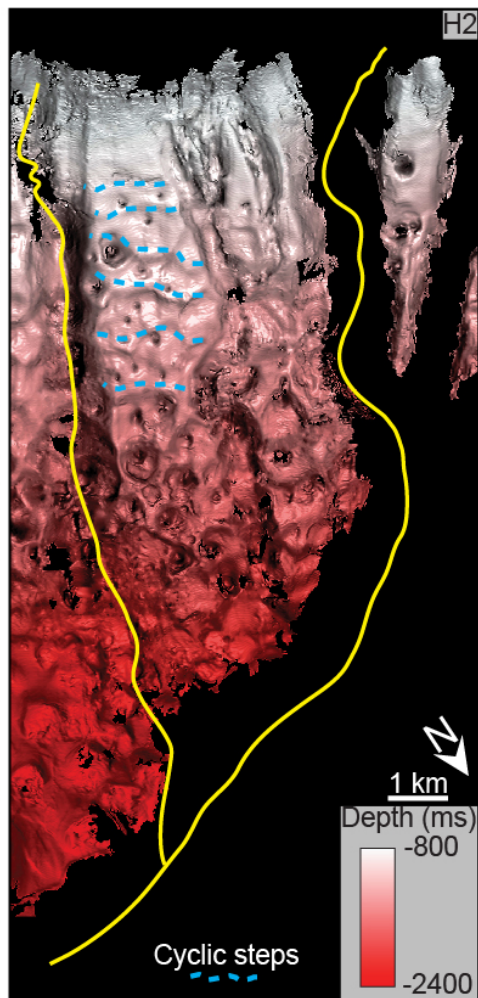
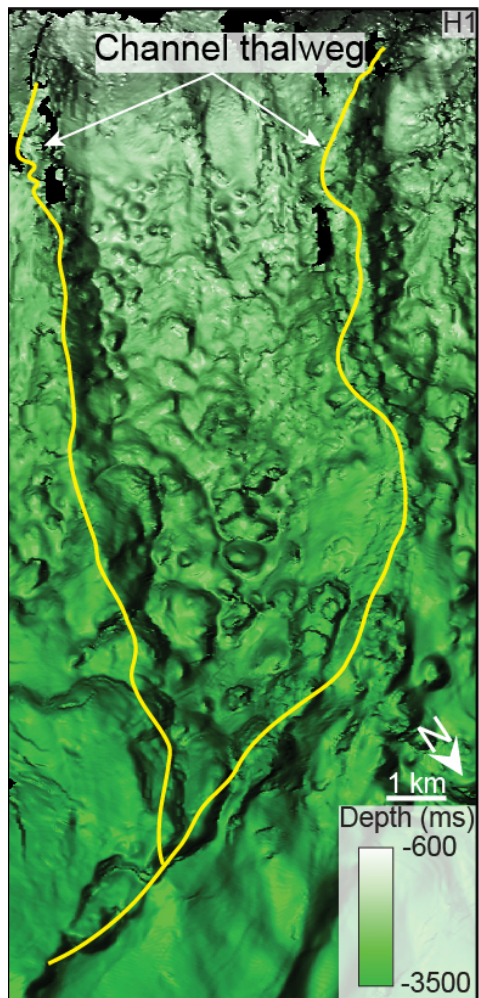
398 **Figure 6.** Schematic sketch illustrating a possible evolution of stacked sediment waves, migrating  
399 upslope and creating a permeable preferential path for upward fluid flow. See text for explanation.  
400 Acronyms as in Figure 2.

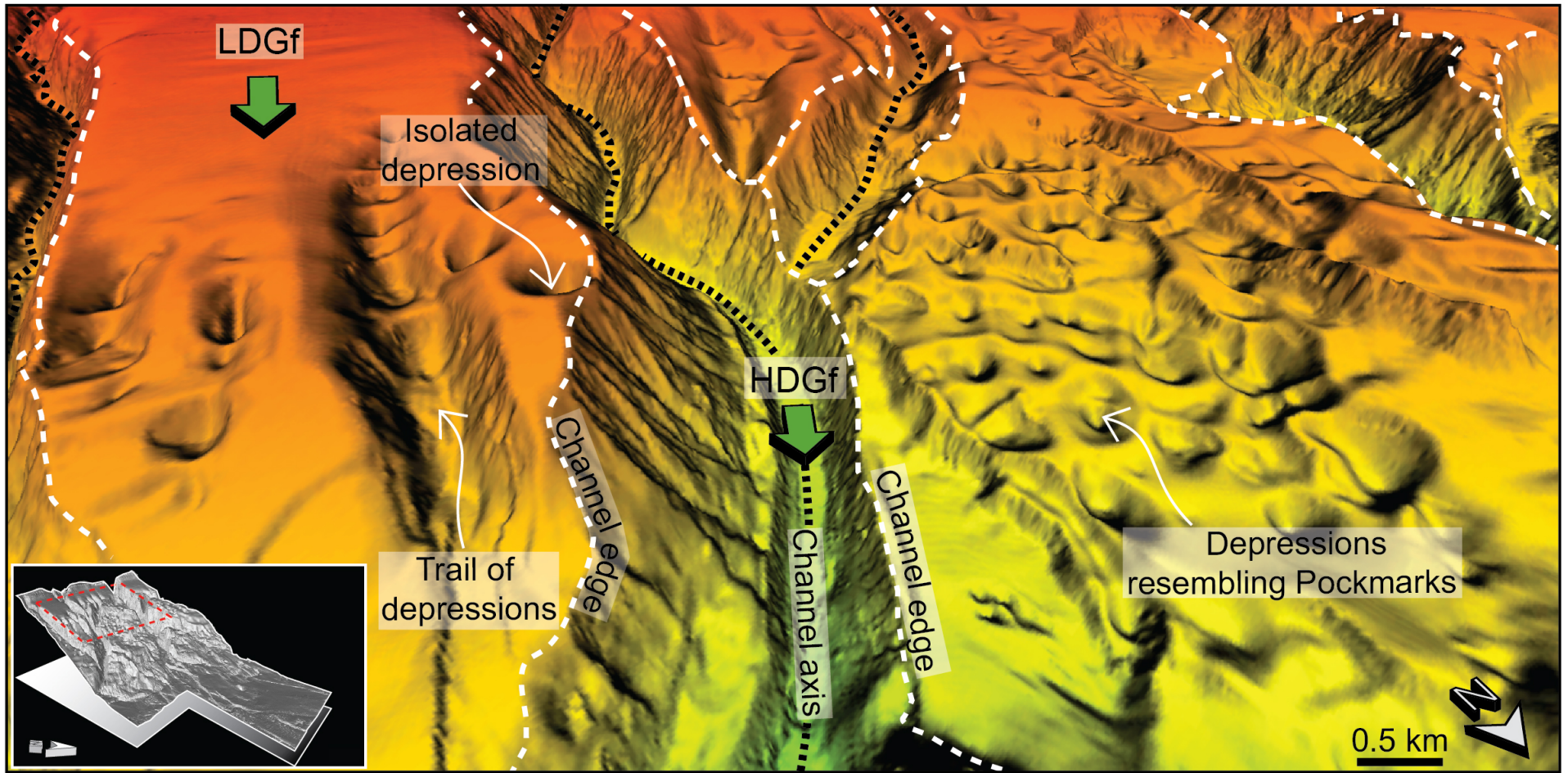
401

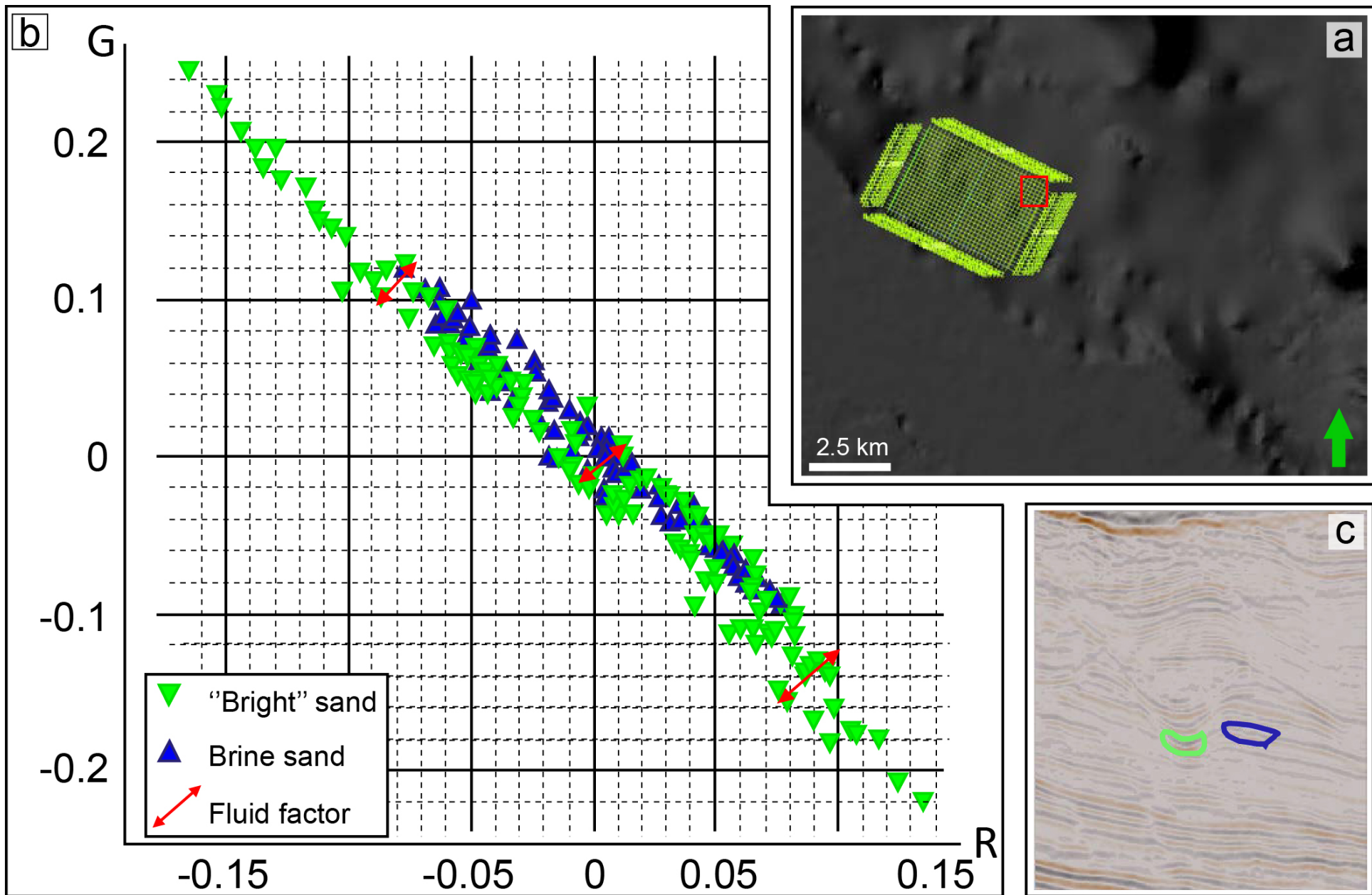


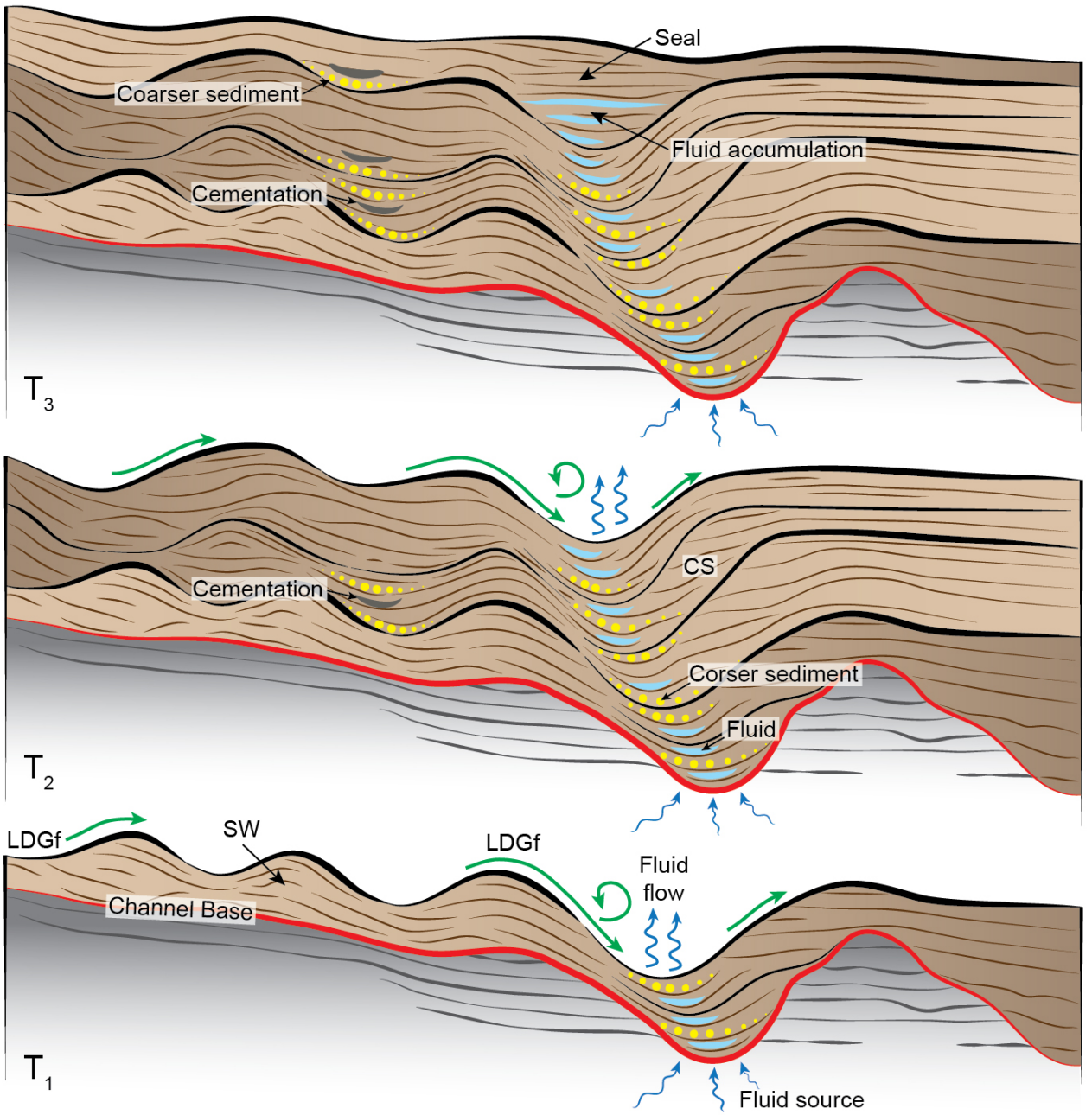
-  Ceará 3D dataset
-  Study area
-  CES-112 Available well
-  Basin and sub-basin boundary
- RFZ Romanche Fracture Zone
- MP Malvinas Plateau
- MAR Mid-Atlantic Ridge













## Supplementary material

### AVO using partial stack.

Partial stacked data provided by CGG have been used to explore some qualitative amplitude analysis in the area of interest. The partial stack data processed and released by CGG (Fig. 1) is characterized by near middle and far reprocessed stack data. The data have been processed using an amplitude preservation processing that included geometric spreading corrections and preserved amplitude pre-stack time migration (PSTM). The character of the wavelet discovered during the well analysis was used to correct the Near stack to zero phase. In order to use pre stack data for amplitude versus offset analysis a seismic data condition workflow was necessary to reduce the Noise in the P wave in the form of wavelet variation and the residual NMO biased information.

*Seismic data conditioning workflow:*

The following steps were key to the analysis:

- Phase differences: this is produced by generating peak and through volumes and comparing them and minimizing the difference. The phase was corrected by designing and applying matching filters to match the far stack to the near stack.
- Bedform stack analysis: a bedform indicator attributes for each partial stack groups was applied and then combined
- Frequency changes : instantaneous frequency were calculate for the partial stack volume and compared using the following algorithm :

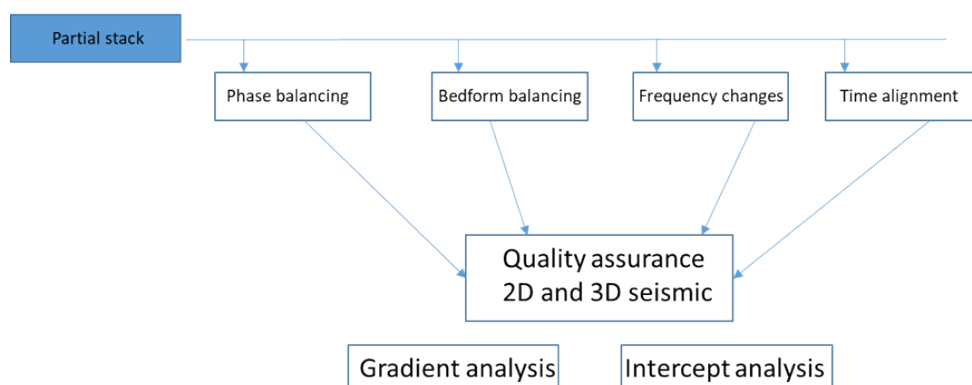
$$(((im1>0)\&(im2>0))*(im2-im1))$$

Where im1 and im2 represent the two main partial stack volumes in analysis

- A Time Alignment – time shifts misalignments are corrected.

As an initial test, a small subset was extracted from the partial stacks for testing of different Seismic Data Conditioning algorithm and the seismic data conditioning workflow was applied to correct for phase, frequency, amplitude and time differences. Once the exact procedure was outlined and tested, the workflow was applied and reviewed throughout the entire volume

### Seismic data conditioning scheme



*AVO analysis:*

Once the near medium and far reflectivity dataset have been QC using the workflow procedure described above they are analysed with the target of calculating the gradient and intercept.

Gradient and intercept from partial stack are calculated using the following expressions:

$$\text{Gradient:} = \frac{R(\theta_f) - R(\theta_n)}{(\sin\theta_f^2 - \sin\theta_n^2)}$$

$$\text{Intercept:} = R(0) = R(\theta_n) - \text{Gradient} * (\sin\theta_n^2)$$

The angles  $\theta_n$  and  $\theta_f$  represents the near and far angle stacks (in our case values are 5 and 15) and the values are plotted across gradient versus intercept volume.